

# High-fidelity preparation, gates, memory and readout of a trapped-ion quantum bit

T. P. Harty,<sup>1</sup> D. T. C. Allcock,<sup>1</sup> C. J. Ballance,<sup>1</sup> L. Guidoni,<sup>1,2</sup>  
H. A. Janacek,<sup>1</sup> N. M. Linke,<sup>1</sup> D. N. Stacey,<sup>1</sup> and D. M. Lucas<sup>1</sup>

<sup>1</sup>*Department of Physics, University of Oxford, Clarendon Laboratory, Parks Road, Oxford OX1 3PU, U.K.*

<sup>2</sup>*University of Paris Diderot, Sorbonne Paris Cité,*

*Laboratoire Matériaux et Phénomènes Quantiques, UMR 7162 CNRS, F-75205 Paris, France*

(Dated: 6 Mar 2014)

The great potential of quantum computing requires two essential ingredients for its realization: high-fidelity quantum logic operations and a physical implementation which can be scaled up to large numbers of quantum bits [1]. We introduce a trapped-ion qubit stored in ultra-stable “atomic clock” states of  $^{43}\text{Ca}^+$ , in which we implement all single-qubit operations with fidelities sufficient for fault-tolerant quantum computing. We measure a combined qubit state preparation and single-shot readout fidelity of 99.93%, a memory coherence time of  $T_2^* = 50$  seconds, and an average single-qubit gate fidelity of 99.9999%. These results are achieved in a room-temperature device without the use of magnetic field shielding or dynamic decoupling techniques to overcome technical noise. The surface-electrode ion trap chip incorporates integrated resonators and waveguides for coherent manipulation of the qubit using near-field microwaves [2]. Two-qubit gates [3] and individual qubit addressing [4] have already been demonstrated using this approach, which is scalable for a many-qubit architecture.

Amongst the candidate technologies for implementing quantum information processing, individual trapped ions were early recognized as a very promising system [5–7]: the qubits are stored in internal atomic energy levels of the ions, which can be extremely stable and well isolated from the environment, and the strong Coulomb interaction between neighbouring ions can be used to mediate qubit-qubit logic. Since the first proposals, multiple-qubit algorithms have been demonstrated [8], and there has been significant progress in developing scalable ion trap technologies [9]. Long qubit memory coherence time [10], high-fidelity state preparation and readout [11], and single-qubit gates with fault-tolerant error rates [12] have all been demonstrated, in a variety of different trapped ions and experiments. In this Letter, we demonstrate all single-qubit operations (preparation, memory, gates and readout) with performances comparable to or better than previous work, and all in the same system. All errors are more than an order of magnitude below the  $\approx 1\%$  fault-tolerant thresholds emerging from recent numerical calculations using surface-code error correction [13]; this is critical for the practical imple-

mentation of fault-tolerant methods, whose resource requirements increase dramatically for error rates close to threshold [14]. Furthermore, the ion-qubit is trapped in a microfabricated surface-electrode trap [15] with a two-dimensional electrode layout which is extendable to large arrays of multiplexed traps, as envisaged in the original proposal for scalable trapped-ion quantum information processing [7]. We describe below the trap and the  $^{43}\text{Ca}^+$  qubit, and three experiments performed to measure the combined state preparation and readout error, the qubit coherence time, and the average single-qubit gate error.

The ion trap is of a novel design which incorporates integrated microwave circuitry (resonators, waveguides, and coupling elements), designed to allow single- and two-qubit quantum logic gates to be driven by near-field microwaves [3] instead of by lasers: this will enable all the coherent qubit operations to be performed by electronic techniques, where one can take advantage of readily available microwave sources whose power and absolute frequency are very stable, and which can be easily connected to the trap electrodes. In contrast to solid-state qubit technologies [16], it is not necessary to cool the apparatus to milli-Kelvin temperatures, as the microwave control fields are classical: only the qubits themselves need to be cold, and this is straightforwardly achieved using Doppler laser-cooling. A schematic diagram of the trap and the laser beam layout is shown in figure 1a; the trap is described in more detail in ref. [2].

A single  $^{43}\text{Ca}^+$  ion is loaded into the trap from a 12%-enriched calcium source using isotope-selective photo-ionization [17], and Doppler-cooled with lasers operating at 397 nm and 866 nm. Further lasers at 393 nm, 850 nm and 854 nm are used for qubit readout and reset. An advantage of the  $\text{Ca}^+$  ion is that all wavelengths are available from solid-state diode lasers without the need for frequency-doubling, are compatible with integrated optics [18], and do not cause observable charging of the trap structure under normal operation. The optical operations (laser-cooling, state preparation and readout) are robust to laser intensity and frequency noise (laser linewidths are  $\approx 1$  MHz), and only require low-power beams.

Hyperfine states in the ground  $4S_{1/2}$  level of the ion are used for the qubit states (figure 1b). As spontaneous decay rates are negligible, these states have essentially infinite  $T_1$  times (limited in practice by the ion trapping

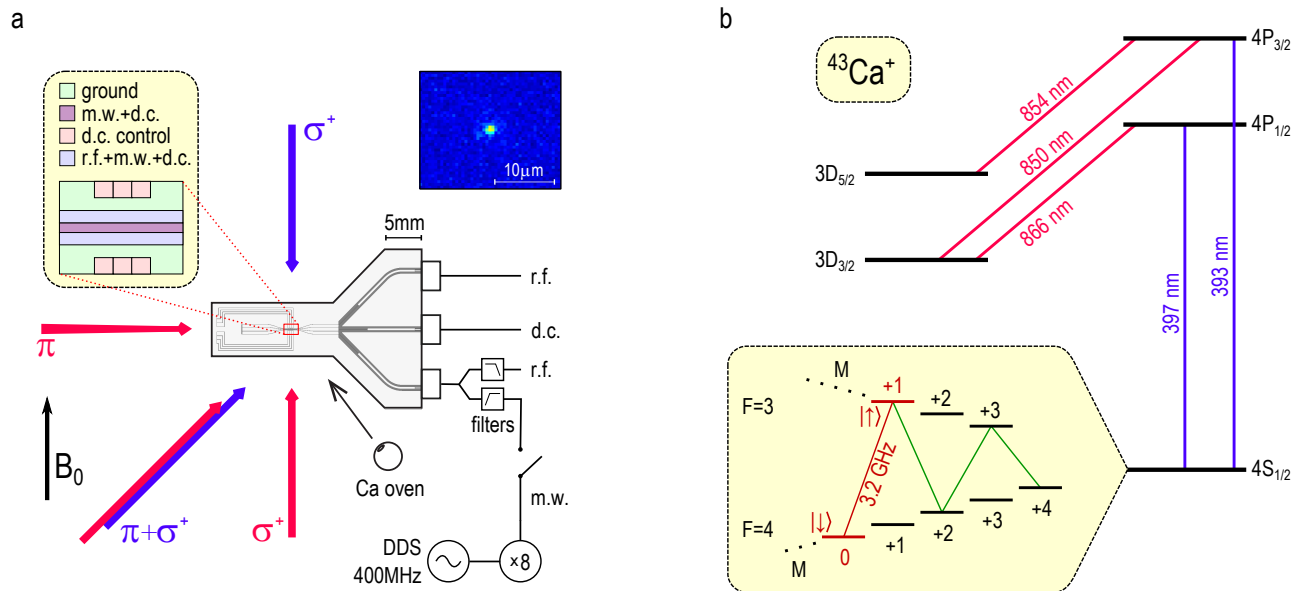


FIG. 1: The ion trap and the qubit. (a) Schematic diagram of the surface ion trap, showing (inset) central electrode layout. Microwave (m.w., 3.2 GHz) signals are combined with the trap radiofrequency voltage (r.f., 40 MHz) via filters; in the experiments reported here, microwaves were only applied to the lower axial electrode. Also shown are laser beam directions and polarizations with respect to the static magnetic field  $B_0 = 146$  G. The violet 397 nm Doppler-cooling beam is elliptically polarized such that it contains only  $\pi$  and  $\sigma^+$  polarizations, and co-propagates with infra-red repumping beams. Circularly  $\sigma^+$  and linearly  $\pi$  polarized beams are used for state preparation and readout as described in Methods (the  $\pi$  beam is at  $\sim 45^\circ$  to the plane of the figure and reflects off the trap surface). To load the trap, neutral Ca atoms effusing from the oven are ionized by laser beams at 423 nm and 389 nm which co-propagate with the Doppler-cooling beams. Ion fluorescence is collected by an imaging system perpendicular to the plane of the trap; the inset shows an image of a single  $^{43}\text{Ca}^+$  ion, which is trapped  $75 \mu\text{m}$  above the electrodes. (b)  $^{43}\text{Ca}^+$  level structure, showing optical transitions used for Doppler cooling, qubit state preparation and readout. The inset shows part of the ground level hyperfine structure, labelled by quantum numbers  $F$  and  $M$ , with the qubit  $|\downarrow\rangle$  and  $|\uparrow\rangle$  states, the 3.2 GHz qubit transition (red) and the auxiliary transitions (green) used for state preparation and readout. The Zeeman splittings between adjacent  $M$  states are  $\approx 50$  MHz.

lifetime, which is typically several hours in this trap under ultra-high vacuum conditions,  $< 10^{-11}$  torr).  $T_2$  coherence times are limited by the frequency stability of the qubit transition. The state energies depend on the static magnetic field  $B$  through the Zeeman effect and ambient magnetic field noise would normally limit the coherence time to a few ms. However, certain transition energies become independent of magnetic field to first order at particular values of the field, due to the non-linear dependence arising from hyperfine state mixing, and these permit particularly stable qubits [10]. We choose one of these so-called “atomic clock” transitions,  $S_{1/2}^{4,0} \leftrightarrow S_{1/2}^{3,+1}$  (where the superscripts denote angular momentum quantum numbers  $F, M$ ), which in  $^{43}\text{Ca}^+$  is field-independent at  $B_0 \approx 146$  G (figure 2a).

The relatively large magnetic field leads to a complex atomic level structure, with Zeeman splittings spanning  $\sim 500$  MHz, and because of the low-lying D levels in  $\text{Ca}^+$  there is no closed cycling transition for laser cooling. We have nevertheless identified a simple Doppler cooling method which requires only two 397 nm frequen-

cies, a single 866 nm frequency, moderate laser powers ( $\sim 100 \mu\text{W}$ ) and a single beam direction. We obtain a fluorescence count rate comparable to that from a single, saturated,  $^{40}\text{Ca}^+$  ion, at  $50\,000 \text{ s}^{-1}$  with a net photon detection efficiency of 0.3%, which is sufficient for high-fidelity fluorescence detection.

To measure the combined state preparation and measurement (SPAM) error we repeatedly prepare the same qubit state, and read it out, averaging over preparations of the  $|\downarrow\rangle$  and  $|\uparrow\rangle$  states (see Methods). For 150 000 preparations of each qubit state, we measure the combined SPAM error to be  $6.8(5) \times 10^{-4}$  (figure 3). As the qubit readout method is not a quantum non-demolition measurement, we cannot repeat it many times to separate the preparation and readout errors, but from estimates of the various contributions to the combined error (table I) we assign errors of  $\approx 2 \times 10^{-4}$  to the state preparation and  $\approx 5 \times 10^{-4}$  to the readout. The error contributions could all be reduced by technical improvements (such as increasing the photon detection efficiency [11]), except for the optical pumping transfer to  $D_{5/2}$  which is limited to

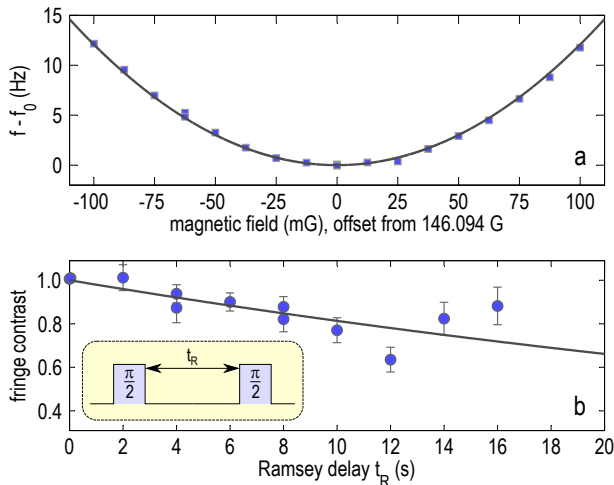


FIG. 2: (a) Microwave spectroscopy of the qubit transition, varying the static magnetic field  $B$  through the field-independent point  $B_0 = 146.094$  G. At each field value, the qubit transition frequency  $f$  was measured by Ramsey spectroscopy, to a precision  $\approx 0.1$  Hz. The field-independent qubit transition is at  $f_0 = 3\,199\,941\,077$  Hz after adjusting for a  $-5$  Hz a.c. Zeeman shift due to r.f. currents in the trap electrodes. The solid line shows the expected frequency calculated using the Breit-Rabi formula assuming the known zero-field hyperfine splitting [30] and a nuclear magnetic moment [19] of  $\mu_I = -1.31535\mu_N$ . (b) Qubit coherence time measurements. At each value of the Ramsey free precession time  $t_R$  the phase of the second  $\pi/2$  pulse was varied to produce a set of Ramsey fringes. The contrast of the fringes is fitted with an exponential decay, giving a coherence time  $T_2^* = 50(10)$  s.

a minimum error [19] of  $\approx 1 \times 10^{-4}$  (at  $B_0 = 146$  G) by the atomic structure of  $^{43}\text{Ca}^+$ .

The qubit coherence time was measured by performing Ramsey experiments (without any dynamic decoupling pulses [20]) on the  $S_{1/2}^{4,0} \leftrightarrow S_{1/2}^{3,+1}$  qubit transition at  $f_0 = 3.200$  GHz (see Methods). Ramsey delays up to  $t_R = 16$  sec were used, with results shown in figure 2b. An exponential decay fitted to the data gives a coherence time  $T_2^* = 50(10)$  sec. The coherence time may be limited by residual magnetic field drift (the qubit's second-order field dependence is  $d^2f/dB^2 = 2.4$  mHz/mG<sup>2</sup>), instability of the local oscillator, and fluctuations in the amplitude of the trap r.f. voltage (we measure an a.c. Zeeman shift of  $-5$  Hz in the qubit frequency due to the effect of r.f. currents in the trap electrodes [21]). The reduction in fringe contrast could also be due to effects unrelated to the qubit coherence, for example heating of the ion during  $t_R$  which increases readout error due to Doppler-broadening of the 393 nm shelving transition. We note that longer coherence times have been measured in large ensembles, using trapped ions [22] and nuclear spins [23] (in the latter case, only with multiple dynamical decoupling pulses).

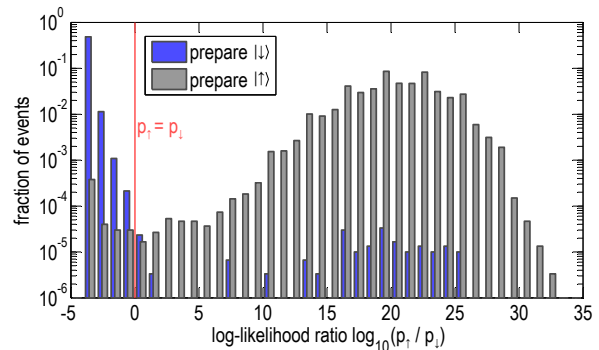


FIG. 3: Qubit state preparation and measurement (SPAM) results. We prepared and measured the  $|\downarrow\rangle$  (blue histogram) and  $|\uparrow\rangle$  (grey histogram) qubit states 150 000 times each, as described in Methods. For each measurement the likelihood  $p_\downarrow$  (or  $p_\uparrow$ ) that the state was  $|\downarrow\rangle$  (or  $|\uparrow\rangle$ ) was calculated from the time-resolved photon counts detected on a photomultiplier (see [11]); if  $p_\uparrow > p_\downarrow$  we infer that the qubit was in the  $|\uparrow\rangle$  state, and vice versa. If the state inferred disagrees with the state prepared, either a preparation or a measurement error has occurred; thus the fraction of experiments in which an error occurred is given by the sum of the blue events above the  $p_\uparrow = p_\downarrow$  threshold ( $2 \times 10^{-4}$ ) and the grey events below threshold ( $5 \times 10^{-4}$ ).

The fidelity of single-qubit gates driven by one of the near-field integrated microwave electrodes was measured by the technique of randomized benchmarking [24], which yields an average gate error appropriate to a computational context. We use the same method as ref.[12], which reports the previous lowest single-qubit gate error. Having prepared the qubit in  $|\uparrow\rangle$ , we apply a pre-programmed pseudo-random sequence of logical gates, where each logical gate comprises a Pauli gate followed by a Clifford gate. The sequence terminates by rotating the qubit into either  $|\downarrow\rangle$  or  $|\uparrow\rangle$ , chosen with equal probability. Clifford gates are randomly chosen to rotate the qubit about the  $\pm x$  or  $\pm y$  axes on the Bloch sphere; Pauli gates are randomly chosen to rotate about the  $\pm x$ ,  $\pm y$  or  $\pm z$  axes, or to be a  $\pm I$  identity gate. In the experiment, each Clifford gate is performed by a microwave  $\pi/2$ -pulse and each Pauli gate by a pair of  $\pi/2$ -pulses. Identity gates are implemented using delays of the same duration ( $12 \mu\text{s}$ ) as the  $\pi/2$ -pulses,  $\pm z$  rotations as an identity followed by a rotation of the logical frame of the qubit for subsequent pulses. The microwaves are generated by a frequency-octupled 400 MHz direct digital synthesis (DDS) source, fed via a switch to one of the m.w. electrodes (figure 1a); the enhancement provided by the integrated m.w. resonator and the proximity of the ion to the electrode means that a low m.w. power (0.1 mW) is sufficient and a power amplifier is not necessary. The m.w. power was periodically calibrated during the experiments using a sequence of 751  $\pi/2$ -pulses. The qubit was kept at the field-independent point by servoing the magnetic field as



crowave  $\pi$ -pulses on the transitions indicated in figure 1b then transfers the ion to the  $|\uparrow\rangle$  (or  $|\downarrow\rangle$ ) qubit state, as desired.

**State readout:** To read out the qubit state, a state-selective optical pumping method is used to implement the transfer  $(|\downarrow\rangle, |\uparrow\rangle) \rightarrow (4S_{1/2}^{3,+1}, 3D_{5/2})$ , followed by fluorescence detection. First, three microwave  $\pi$ -pulses transfer population in  $|\uparrow\rangle$  to  $S_{1/2}^{4,+4}$ , and a fourth  $\pi$ -pulse transfers  $|\downarrow\rangle \rightarrow S_{1/2}^{3,+1}$ . Population in  $S_{1/2}^{4,+4}$  is then “shelved” in the metastable  $3D_{5/2}$  level by a repeated sequence of (393 nm  $\sigma^+$ , 850 nm  $\sigma^+$ , 850 nm  $\pi$ ) pulses, as described in [11]; this shelving method is more involved than readout in ions without low-lying D levels, but more robust to imperfections in laser polarizations. Finally the 397 nm and 866 nm Doppler-cooling lasers are applied again and we detect whether or not the ion was shelved by the absence or presence of 397 nm fluorescence. Time-resolved photon counting is used to discriminate against spontaneous decays from the  $D_{5/2}$  level during the detection period [11].

**Coherence time measurements:** The microwave  $\pi/2$ -pulses are derived from a local oscillator referenced to an atomic clock with a nominal stability of  $< 10^{-11}$  (accuracy and long-term stability were verified by comparison with GPS [19]). We measure the contrast of Ramsey interference fringes as the Ramsey delay time  $t_R$  is increased (figure 2b) for delays up to 16 sec. These measurements are demanding on the stability of experimental conditions since, with a single qubit, each data point requires several hundred Ramsey experiments. To ensure that the applied magnetic field remains close to the field-independent point, the frequency of the field-dependent  $S_{1/2}^{4,+4} \leftrightarrow S_{1/2}^{3,+3}$  transition is periodically measured by the computer controlling the experiment, and an appropriate correction is applied to the magnetic field coil current.

## ACKNOWLEDGEMENTS

It is a pleasure to thank E. Knill and A. Meier for advice regarding the randomized benchmarking experiment, and A. Steane and J. Jones for helpful discussions. This work was supported by the Engineering and Physical Sciences Research Council (EPSRC) via the Quantum Coherence Science and Innovation network.

## AUTHOR CONTRIBUTIONS

T.P.H., D.T.C.A., C.J.B. and D.M.L. built the apparatus, designed and performed experiments, analysed data and wrote the paper. L.G. assisted with building apparatus and preliminary experiments. H.A.J. and D.N.S. simulated the atomic system. N.M.L. analysed data and produced the figures. All authors discussed the results and the text of the manuscript.

- 
- [1] M. A. Nielsen and I. L. Chuang, *Quantum computation and quantum information* (Cambridge University Press, 2000).
  - [2] D. T. C. Allcock *et al.*, Appl. Phys. Lett. **102**, 044103 (2013).
  - [3] C. Ospelkaus *et al.*, Nature **476**, 181 (2011).
  - [4] U. Warring *et al.*, Phys. Rev. Lett. **110**, 173002 (2013).
  - [5] J. I. Cirac and P. Zoller, Phys. Rev. Lett. **74**, 4091 (1995).
  - [6] A. Steane, Appl. Phys. B **64** (1997).
  - [7] D. J. Wineland *et al.*, J. Res. NIST **103**, 259 (1998).
  - [8] R. Blatt and D. Wineland, Nature **453** (2008).
  - [9] C. Monroe and J. Kim, Science **339**, 1164 (2013).
  - [10] C. Langer *et al.*, Phys. Rev. Lett. **95**, 060502 (2005).
  - [11] A. H. Myerson *et al.*, Phys. Rev. Lett. **100**, 200502 (2008).
  - [12] K. R. Brown *et al.*, Phys. Rev. A **84**, 030303 (2011).
  - [13] A. G. Fowler *et al.*, Phys. Rev. A **86**, 03232 (2012).
  - [14] A. M. Steane, Phys. Rev. A **68**, 042322 (2003).
  - [15] S. Seidelin *et al.*, Phys. Rev. Lett. **96**, 253003 (2006).
  - [16] M. H. Devoret and R. J. Schoelkopf, Science **339**, 1169 (2013).
  - [17] D. M. Lucas *et al.*, Phys. Rev. A **69**, 012711 (2004).
  - [18] G. R. Brady *et al.*, Appl. Phys. B **103**, 801 (2011).
  - [19] T. P. Harty, D.Phil. thesis, University of Oxford (2013).
  - [20] D. J. Szwer *et al.*, J. Phys. B **44**, 025501 (2011).
  - [21] D. J. Berkeland *et al.*, Phys. Rev. Lett. **80**, 2089 (1998).
  - [22] J. J. Bollinger *et al.*, IEEE Trans. Instr. Meas. **40**, 126 (1991).
  - [23] K. Saeedi *et al.*, Science **342**, 830 (2013).
  - [24] E. Knill *et al.*, Phys. Rev. A **77**, 012307 (2008).
  - [25] D. P. L. Aude Craik *et al.*, Appl. Phys. B **114**, 3 (2014).
  - [26] M. H. Levit, Prog. Nucl. Magn. Reson. Spectrosc. **18**, 61 (1986).
  - [27] C. J. Ballance *et al.*, in preparation (2014).
  - [28] J. Benhelm *et al.*, Nature Physics **4**, 463 (2008).
  - [29] G. Kirchmair *et al.*, Phys. Rev. A **79**, 020304 (2009).
  - [30] F. Arbes *et al.*, Z. Phys. D **31**, 27 (1994).